A numerical control algorithm for a B-double truck-trailer with steerable trailer wheels and active hitch angles

Andrew Percy[1] and

Ian Spark[2]

[1]Corresponding author. Address: Monash University, SASE, Northways Road, Churchill, Victoria, Australia, 3842. Email: andrew.percy@monash.edu.au

[2]Gippsland Regional Automation Centre, Monash University, Austrailia.

Abstract

This paper presents a new algorithm for the control of a B-double truck-trailer with steerable trailer wheels and active hitch angles, designed to minimize both off-tracking and scuffing. Each trailer has six autonomously steered double wheels, although each double wheel is modelled by a centrally placed single wheel. Each hitch point, joining truck to first trailer and first trailer to second trailer, as well as a nominated point central to the axles of the second trailer, traverses the same path which is determined by an operator controlling the path curvature and truck speed. The algorithm approximates the ideal solution in which all wheels on each trailer have the same centre of curvature. The actively controlled hitch angles, satisfying the path following constraints, provide a further level of cooperative redundancy of steering systems. Simulations are carried out to show the effects of changing curvature and front hitch speed on hitch path, wheel angles, and hitch angles as well as the accuracy of the algorithm. Further simulation is carried out to show the improvement in off-tracking of the new control system over current B-double fixed wheel systems.

KEYWORDS: B-double truck-trailer, control system, off-tracking, cooperative redundancy.

1 Introduction

This paper gives a control system for a B-double truck-trailer vehicle traversing a path which is determined in real-time by the truck's operator. A numerical algorithm is used to compute the first and second trailer wheel angles. The objective of this control system is to minimize both scuffing and off-tracking of the trailer wheels. Scuffing is the movement of a tyre contact patch relative to the ground, perpendicular to the plane of the wheel, and results in tyre wear. Scuffing is minimized by ensuring the plane of the wheel is in the direction of the wheels motion. Off tracking is where wheels that have the same path when the vehicle is traveling in a straight line, follow different paths when the vehicle is moving in a curved path and results in "cutting of corners". The algorithm also computes the hitch-angles between the truck and first trailer and between the two trailers and active control of these angles provides a cooperative redundancy of two steering systems, with the advantage that when one system begins to fail it is backed up by the other system. Typical dimensions of a B-double are shown in Figure 1.

This paper gives details of the control calculations and also provides simulation studies to demonstrate the effectiveness of the system. For an experimental test-bed, electric screw actuators are suggested for the manipulation of wheel angles once the optimal angle has been calculated. The hitch angle actuator would need to exert more force than the wheel

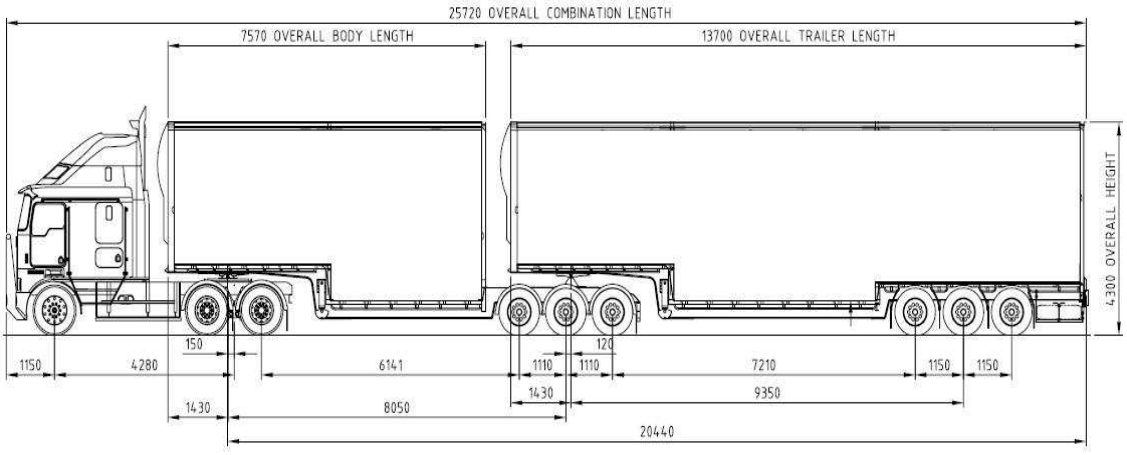

Figure 1: Typical dimensions, of a B-double truck-trailer vehicle. Lengths are in mm.

angle actuator, so a hydraulic actuator would be more suitable. Both types of actuators can be operated either internally or externally [1] to the truck so that parking or reversing of the vehicle may be done by external remote control with the operator able to move around and get a better view of the vehicle. Reversing the vehicle will not be covered in this paper.

Hydraulic actuators are used to steer heavy articulated vehicles in mining and construction, such as articulated wheeled loaders and articulated dump trucks. Research to optimize the effectiveness of these systems [2, 3] and to control them externally "by wire" [4] is on-going.

In a series of papers [5, 6, 7, 8] a control algorithm for a snake-like robot has been developed in which each segment of the robot has autonomous 4 wheel drive and 4 wheel steering, and each hitch point between segments follows the same path as the front hitch.

This numerical algorithm has been modified and improved to be applied to a B-double truck-trailer. In particular, the B-double truck-trailer does not consist of a linked series of identical, symmetrical segments. The truck (prime mover) does not have steerable rear wheels and, as a result, determination of the path of the vehicle required new equations. Minor improvements have occurred as a natural part of the modelling process, such as a loosening of initial/boundary conditions which allow the path to be determined from a "standing start" rather than requiring a constant, non-zero speed in the initial stage.

Firstly, the path traveled by the hitch joining the truck to the first trailer must be determined given the instantaneous input from the operator, at time t, of the truck's steerable wheel angles, $\alpha(t)$, and velocity, $v(t)$, of the central point of the truck's rear axles (denoted (x, y) in Figure 2). The instantaneous radius of curvature, $\frac{1}{\kappa(t)}$, is the radius of the circle best fitting the curved path locally to a given point and can be determined as a function of $\alpha(t)$. Negative κ indicates a right turn, $\kappa = 0$ indicates no turn and $\kappa > 0$ indicates a left turn. From the path of (x, y), the path and velocity of the truck hitching point can be determined. Figure 1 shows that typically the hitch point is 150 mm in front of (x, y).

Once the path of the truck hitching point has been determined, knowing the length of each trailer allows the position, on that path, of the second hitch point (between trailers) and a central point of the rear trailer's axles be found (the points (x_2, y_2) and (x_3, y_3) respectively, on Figure 4). The choice of having these points designated as following the same path is quite arbitrary (any points could be chosen to follow the path) but presumed

the most sensible choice to reduce off-tracking. For simplicity, the point (x_3, y_3) will be called the "third hitching point", as the algorithm generalizes to road trains with more than two trailers. There is then enough information to calculate wheel angles in a number of ways. In the literature, the of use of kinematic, dynamic or hybrid system approaches, perhaps with feedback [9, 10, 11, 12] tends to neglect calculating time or use constant curvature path tracking, splines (for example [13]), or specific predetermined maneuvers such as lane changing. These approaches generally have a common constraint that the front to rear, central axis be tangential to the path, and this is inconsistent with the constraint that all hitch points follow the same path.

The geometrical control system given in [8] assumes wheels have no slip (movement of a tyre contact patch relative to the ground, parallel to the plane of the wheel) and calculates "effective wheel angles" by also neglecting the slip angle associated to pneumatic tyres. When any rolling wheel is subjected to a side (or cornering) force, the effective rolling direction will differ slightly from the apparent rolling direction. This difference is termed the slip angle. For small cornering forces the slip angle tends to be proportional to the cornering force. However as the cornering force approaches its limit the variation of slip angle becomes non linear. Once the maximum cornering force has been reached the slip angle often increases to very high values as the cornering force decreases. In this case the wheel is skidding and no part of the tyre contact patch is stationary relative to the ground.

In this paper we will be most interested in low speed low radius of curvature turns under which scuffing and off-tracking would be large for fixed axle vehicles. Under these

conditions the cornering force required will be low and the associated slip angles will be negligible. For high speed turns, although the cornering forces will be much larger, the radius of curvature will be large so that the tendency for both off tracking and scuffing will be small. Spark and Ibrahim [14, 15] have proposed two methods of accounting for slip angles in the geometrical calculation of "effective wheel angles". In [14] they deduce the linear elastic portion of the slip angles from measurement of the cornering force and vertical force on each wheel. In [15] they measure the total slip angles with the aid of dummy castors located at opposite ends of each vehicle module. In the latter case only slip angles up to the limit of adhesion are accounted for.

The geometrical control system calculates a common centre of curvature (COC) for the six wheels and two hitch points of each trailer. Using a similar geometry to [5], the wheel angles can be given as functions of R_x and R_y, the scalar components of the vector from the hitch points to the COC, perpendicular and parallel to the inter-hitch axis of each trailer. The geometry in [5] required the calculation of an additional vector from the segments central point (itself calculated from the hitch points) to the COC and eliminating this calculation has increased the algorithm's speed.

Since the calculation of wheel angles and speed takes a finite processing time, the proposed control system samples the operator's values of steerable wheel angle and speed at a fixed time increment. The time increment must be sufficiently long to allow the calculation of the wheel and hitch angles of each trailer before the control parameters are sampled again. At this stage resources to construct a test-bed are not available, however

the use of sensors and global positioning could be used on such a test-bed to minimize calculation time and increase accuracy further.

If the path is too curved situations can develop where the rear hitch of a trailer may equally well travel along the path in a forward or backward direction. This is avoided by restricting $\kappa < \frac{2}{l}$, with l the inter-hitch distance, so that the front and rear hitches cannot be at the ends of a diameter of a circle. Restricting the range of hitch angle values can also be used to prevent this situation occurring and also to prevent jack-knifing.

The equations for wheel angles and hitch point angles are given in Section 2.

Simulations are performed in Section 3 to validate the algorithm, using variable curvature and speed. A comparison of off-tracking with standard fixed wheel B-doubles trailers, on a circular arc, is also simulated and demonstrates the significant improvement achieved with steerable trailer wheels.

2 Calculating the trailer wheel angles and hitch angles

The rear axles of a standard truck (prime mover) are fixed with the wheels non steerable. The centre of curvature for the truck with an Ackerman steering system can be calculated as a point which is a perpendicular length of $\frac{1}{\kappa}$ from the central point of the truck's rear axles (labelled (x, y) in Figure 2). Since $\frac{1}{\kappa}$ is the radius of curvature, κ is the path curvature as defined in differential geometry [16].

Given a nominal wheel placed at the centre of the front axis with a steering angle of

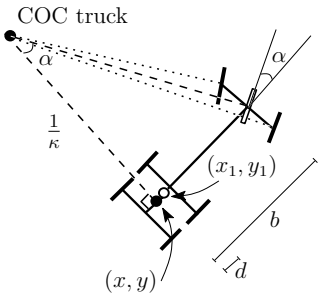

Figure 2: Trucks centre of curvature

α then the relation between the curvature, κ, of the path of (x, y) and the steering angle, is given by $\kappa = \dfrac{\tan\alpha}{b}$, where b is the length from (x, y) to the front axle. It is more natural for the operators steering parameter to be the value of α which is proportional to the rotation of the truck's steering wheel, rather than directly inputting κ which has a non-linear relation to steering wheel rotation. The operator would adjust α to achieve a desired path.

Consider the truck travelling in a plane with the standard orthonormal basis $\mathbf{i}$ and $\mathbf{j}$. Let the tangent to the path, $\mathbf{t}(t)$, make an angle of θ with the direction of $\mathbf{i}$. The left hand diagram of Figure 3 illustrates the vector components in the construction for calculating the path using methods of differential geometry detailed in [8].

Given the operator input of $\alpha(t)$ and $v(t)$, calculate $\kappa(t) = \dfrac{\tan\alpha}{b}$ and hence

$$\theta(t) = \int_0^t v(t)\kappa(t)\ dt, \quad x(t) = \int_0^t v(t)\cos\left(\theta(t)\right)\ dt, \quad y(t) = \int_0^t v(t)\sin\left(\theta(t)\right)\ dt \qquad (1)$$

These equations improve those of [8] by using integration with substitution, eliminating the need to calculate arc length, so that now only 3 equations (rather than 4) are needed

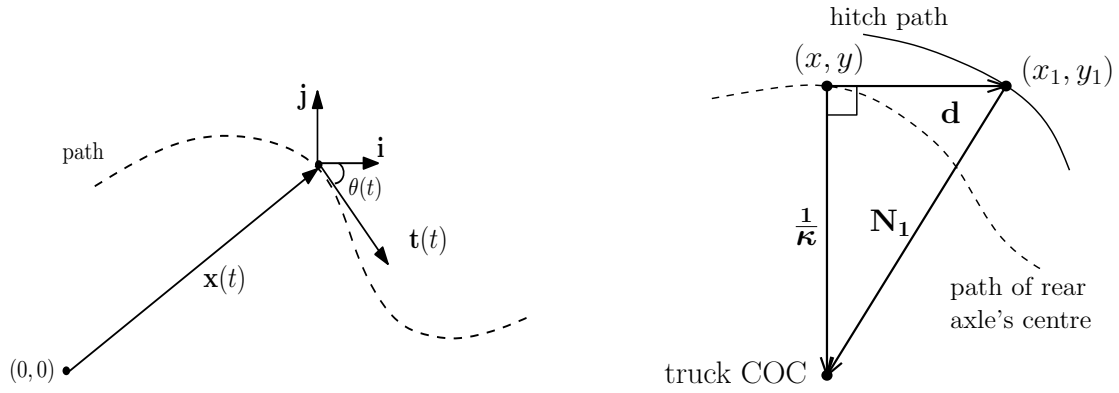

Figure 3: Vector construction for calculating the path $(x(t), y(t))$ (on the left) and the normal to the hitch path (on the right)

to calculate $x(t)$ and $y(t)$, improving the algorithm speed.

From Figures 2 and 3 (left diagram), the truck hitch point, (x_1, y_1) is a distance d in front of (x, y), in a direction tangential to the path. Hence,

$$x_1(t) \;=\; x(t) + d\cos\left(\theta(t)\right) \qquad\qquad y_1(t) \;=\; y(t) + d\sin\left(\theta(t)\right) \tag{2}$$

give the path, as a function of time, of the truck's hitch point. The truck's hitch point, (x_1, y_1), is chosen to determine the path traversed by the trailing hitch points, rather than taking the path (x, y), both because it is a fixed length, l_1, from the second hitch and because it is the point at which truck hitch angle is calculated. This is a departure from the algorithm of [8] in which the path is analogous to that given by (x, y).

The calculation of the truck's hitch point, will take a finite time on any calculating machine. It is natural then to introduce a fixed time increment, Δt, for sampling the

operator's values of v and α, sufficiently large that all calculations can be made before again sampling the operator's input parameters. Introducing the notation $t_i = i\Delta t$, $i = 0, 1, 2, 3, \ldots$, then given $\alpha(t_i)$ and $v(t_i)$, an iterated loop code is used to perform the calculations to give a discretized version of the hitch path $(x_1(t_i), y_1(t_i))$. The code proceeds to calculate discretized wheel angles and hitch angles for the following trailers.

Initial conditions are necessary to approximate the definite integrals of equations (1). Assume that initially $t_0 = 0$ seconds, $\alpha(t_0) = 0$, $\theta_1(t_0) = 0$ and $x_1(t_0) = y_1(t_0) = 0$, so the hitch is moving in the **i** direction and initially at the origin of the plane.

For any $i > 0$, the i-th sample gives $\kappa\,(t_i) = \frac{\tan\alpha(t_i)}{b}$ and $v\,(t_i)$ and assume the values $\theta(t_{i-1})$, $x(t_{i-1})$ and $y(t_{t-1})$ have previously been calculated. Then trapazoidal approximation of the integrals (1) give equations

$$\begin{aligned}
\theta(t_i) &= \theta(t_{i-1}) + \frac{1}{2}(v(t_i)\kappa(t_i) + V(t_{i-1})\kappa(t_{i-1}))(\Delta t)) \\
x_1(t_i) &= x(t_{i-1}) + \frac{1}{2}\left(v(t_i)\cos\left(\theta(t_i)\right) + v(t_{i-1})\cos\left(\theta(t_{i-1})\right)\right)(\Delta t) + d\cos\left(\theta(t_i)\right) \\
y_1(t_i) &= y(t_{i-1}) + \frac{1}{2}\left(v(t_i)\sin\left(\theta(t_i)\right) + v(t_{i-1})\sin\left(\theta(t_{i-1})\right)\right)(\Delta t) + d\sin\left(\theta(t_i)\right)
\end{aligned}$$

as an iterative computation (suitable for encoding into a loop program initialized with the values at t_0) of the discretized hitch path. By definition of the Riemann integral as $\Delta t \to 0$ these discrete equations converge to the analytical solutions of equations (2).

A tangent vector to this hitch point path is given by $\frac{d}{dt}\mathbf{x_1}(t) = \frac{d}{dt}x_1(t)\ \mathbf{i} + \frac{d}{dt}y_1(t)\ \mathbf{j}$. Applying the fundamental theorem of calculus to equations (1) allows the derivatives of

$x_1(t)$ and $y_1(t)$ to be calculated in terms of the input parameters, giving the tangent

$$\frac{d}{dt}\mathbf{x_1}(t) = [-d\ v(t)\kappa(t)\sin(\theta(t)) + v(t)\cos(\theta(t))]\,\mathbf{i} + [d\ v(t)\kappa(t)\cos(\theta(t)) + v(t)\sin(\theta(t))]\,\mathbf{j}$$

A normal to the path is then

$$\mathbf{N_1}(t) = [d\ v(t)\kappa(t)\cos(\theta(t)) + v(t)\sin(\theta(t))]\,\mathbf{i} - [-d\ v(t)\kappa(t)\sin(\theta(t)) + v(t)\cos(\theta(t))]\,\mathbf{j}$$

and, with some algebraic manipulation, a unit normal to the hitch path at discrete time intervals t_i is

$$\begin{aligned}\hat{\mathbf{N}}_\mathbf{1}(t_i) &= N_{11}(t_i)\mathbf{i} + N_{12}(t_i)\mathbf{j} \\ &= \left[\frac{d\kappa(t_i)\cos\theta(t_i) + \sin\theta(t_i)}{\sqrt{d^2(\kappa(t_i))^2 + 1}}\right]\mathbf{i} + \left[\frac{d\kappa(t_i)\sin\theta(t_i) - \cos\theta(t_i)}{\sqrt{d^2(\kappa(t_i))^2 + 1}}\right]\mathbf{j}\end{aligned}$$

The same equation can be achieved geometrically from Figure 3 (right diagram), under the assumption that an Ackerman steering system results in all points on the truck moving around the same centre of curvature. Some care must be taken with the sign of κ (positive or negative) in this alternative method.

Consequently, each discrete path point has an associated unit normal to the path at that point.

The next step in the calculation is to determine the position of the second and third hitch positions $(x_2(t_i), y_2(t_i))$ and $(x_3(t_i), y_3(t_i))$. The method detailed in [8] finds $(x_2(t_i), y_2(t_i))$ as the discrete point on the path that is closest to the distance l_1 from $(x_1(t_i), y_1(t_i))$. This may be the same point as $(x_2(t_{i-1}), y_2(t_{i-1}))$ or a point in front of it. Successive points

are tested to find the most suitable point. The unit normal associated to the path point $(x_2(t_i), y_2(t_i))$ is denoted $\hat{\mathbf{N}}_\mathbf{2}(t_i)$.

The third hitch point, $(x_3(t_i), y_3(t_i))$, is the discrete path point that is closest to the distance l_2 from $(x_2(t_i), y_2(t_i))$ and has associated unit normal $\hat{\mathbf{N}}_\mathbf{3}(t_i)$.

The centre of curvature of the first trailer, $COC_1(t_i)$, is the intersection of a line from $(x_1(t_i), y_1(t_i))$ in the direction of $\hat{\mathbf{N}}_\mathbf{1}(t_i)$ and the line from $(x_2(t_i), y_2(t_i))$ in the direction of $\hat{\mathbf{N}}_\mathbf{2}(t_i)$. The centre of curvature of the second trailer, $COC_2(t_i)$, is the intersection of a line from $(x_2(t_i), y_2(t_i))$ in the direction of $\hat{\mathbf{N}}_\mathbf{2}(t_i)$ and the line from $(x_3(t_i), y_3(t_i))$ in the direction of $\hat{\mathbf{N}}_\mathbf{3}(t_i)$.

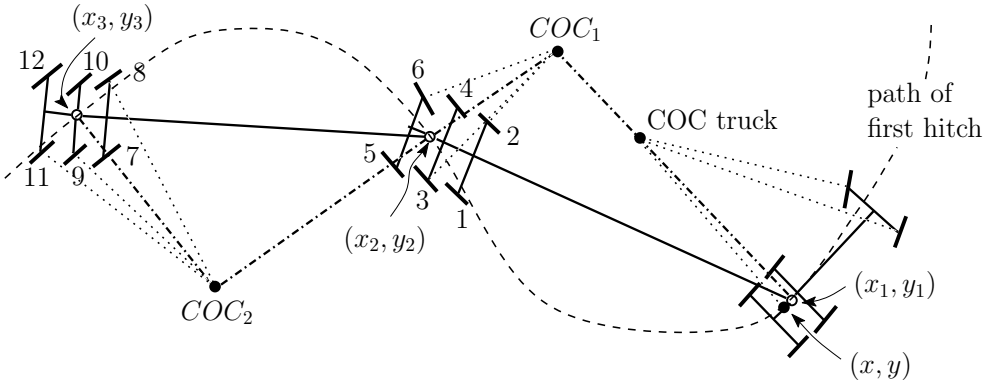

Figure 4: Position of the COC's used to determine wheel angles. Trailer wheels are numbered 1 to 12.

Once the COC's and the hitch points are known, a vector can be calculated from the second hitch point to the COC_1 and the third hitch point to the COC_2. These vectors can then be decomposed into components parallel and perpendicular to the trailers central line

running from second hitch to first and from rear reference to second hitch. The lengths of these components are shown as R_{1y}, R_{1x}, R_{2y} and R_{2x} in Figure 5. Each component will be a function of time, t_i.

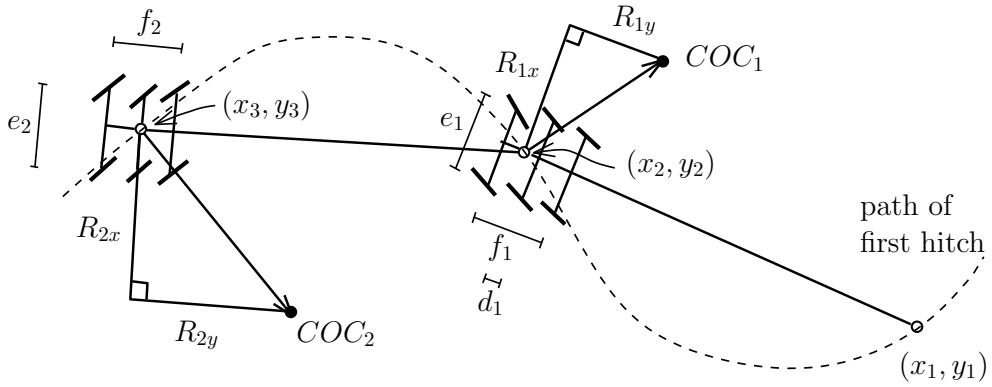

Figure 5: Lengths of COC's perpendicular and parallel to the trailers, with axle dimensions

From the values of R_{1y}, R_{1x}, R_{2y}, R_{2x}, d_1, f_1, e_1, f_2 and e_2 the wheel angles can be calculated by trigonometry as in [5]. However because the values of R_{1y}, R_{1x}, R_{2y} and R_{2x} can become infinite, singularities may occur without the algebraic manipulation performed in [8]. The manipulation involves inverting any quantities that became infinite so the inverted quantity remains finite at all times, and then taking this inversion into account throughout the calculations. It is assumed that $R_{1y} > 0.5f_1 + d_1$ and $R_{2y} > 0.5f_2$ so that all positive wheel angles will indicate anticlockwise rotation and negative angles, clockwise rotation. Angles are calculated in radians but can be converted to degrees in the final step.

In the calculation of the COC's, the lengths of the COC's from the hitch points is

determined, and inverting these quantities we get the finite quantities

$$\begin{aligned}
K_{11}(t_i) &= \frac{N_{11}(t_i)N_{22}(t_i) - N_{21}(t_i)N_{12}(t_i)}{N_{22}\left(x_2(t_i) - x_1(t_i)\right) + N_{21}\left(y_1(t_i) - y_2(t_i)\right)} \\
K_{12}(t_i) &= \frac{N_{11}(t_i)N_{22}(t_i) - N_{21}(t_i)N_{12}(t_i)}{N_{12}\left(x_2(t_i) - x_1(t_i)\right) + N_{11}\left(y_1(t_i) - y_2(t_i)\right)} \\
K_{21}(t_i) &= \frac{N_{21}(t_i)N_{32}(t_i) - N_{31}(t_i)N_{22}(t_i)}{N_{32}\left(x_3(t_i) - x_2(t_i)\right) + N_{31}\left(y_2(t_i) - y_3(t_i)\right)} \\
K_{22}(t_i) &= \frac{N_{21}(t_i)N_{32}(t_i) - N_{31}(t_i)N_{22}(t_i)}{N_{22}\left(x_3(t_i) - x_2(t_i)\right) + N_{21}\left(y_2(t_i) - y_3(t_i)\right)}
\end{aligned} \tag{3}$$

associated to the lengths of the truck hitch to COC_1, the second hitch to COC_1, the second hitch to COC_2 and the rear reference to COC_2.

Then an inverted-compatible form of the coordinates of $COC_1(t_i) = (C_{11}(t_i), C_{12}(t_i))$ and $COC_2(t_i) = (C_{21}(t_i), C_{22}(t_i))$ are given by

$$\begin{aligned}
C_{11}(t_i) &= K_{11}(t_i)x_1(t_i) + N_{11}(t_i) \qquad C_{12}(t_i) = K_{11}(t_i)y_1(t_i) + N_{12}(t_i) \\
C_{21}(t_i) &= K_{21}(t_i)x_2(t_i) + N_{21}(t_i) \qquad C_{22}(t_i) = K_{21}(t_i)y_2(t_i) + N_{22}(t_i)
\end{aligned} \tag{4}$$

Using equations (3) and (4) the inverted-compatible versions of R_{1y}, R_{1x}, R_{2y} and R_{2x}

are given by

$$
\begin{aligned}
T_{1x}(t_i) &= \frac{\begin{array}{r}(C_{11}(t_i) - K_{11}(t_i)x_2(t_i))\,(y_1(t_i) - y_2(t_i)) \\ -\,(C_{12}(t_i) - K_{11}(t_i)y_2(t_i))\,(x_1(t_i) - x_2(t_i))\end{array}}{\sqrt{(x_1(t_i) - x_2(t_i))^2 + (y_1(t_i) - y_2(t_i))^2}} \\
T_{1y}(t_i) &= \frac{\begin{array}{r}(C_{11}(t_i) - K_{11}(t_i)x_2(t_i))\,(x_1(t_i) - x_2(t_i)) \\ +\,(C_{12}(t_i) - K_{11}(t_i)y_2(t_i))\,(y_1(t_i) - y_2(t_i))\end{array}}{\sqrt{(x_1(t_i) - x_2(t_i))^2 + (y_1(t_i) - y_2(t_i))^2}} \\
T_{2x}(t_i) &= \frac{\begin{array}{r}(C_{21}(t_i) - K_{21}(t_i)x_3(t_i))\,(y_2(t_i) - y_3(t_i)) \\ -\,(C_{22}(t_i) - K_{21}(t_i)y_3(t_i))\,(x_2(t_i) - x_3(t_i))\end{array}}{\sqrt{(x_2(t_i) - x_3(t_i))^2 + (y_2(t_i) - y_3(t_i))^2}} \\
T_{2y}(t_i) &= \frac{\begin{array}{r}(C_{21}(t_i) - K_{21}(t_i)x_3(t_i))\,(x_2(t_i) - x_3(t_i)) \\ +\,(C_{22}(t_i) - K_{21}(t_i)y_3(t_i))\,(y_2(t_i) - y_3(t_i))\end{array}}{\sqrt{(x_2(t_i) - x_3(t_i))^2 + (y_2(t_i) - y_3(t_i))^2}}
\end{aligned} \tag{5}
$$

Finally, from equations (5) and the truck dimensions in Figure 5 we get the wheel angles of the first and second trailers as

$$
\begin{aligned}
\phi_1(t_i) &= \arctan\left(\frac{T_{1y}(t_i) - (d_1 + \frac{1}{2}f_1)K_{11}(t_i)}{T_{1x}(t_i) - \frac{1}{2}e_1K_{11}(t_i)}\right) & \phi_7(t_i) &= \arctan\left(\frac{T_{2y}(t_i) - \frac{1}{2}f_2K_{21}(t_i)}{T_{2x}(t_i) - \frac{1}{2}e_2K_{21}(t_i)}\right) \\
\phi_2(t_i) &= \arctan\left(\frac{T_{1y}(t_i) - (d_1 + \frac{1}{2}f_1)K_{11}(t_i)}{T_{1x}(t_i) + \frac{1}{2}e_1K_{11}(t_i)}\right) & \phi_8(t_i) &= \arctan\left(\frac{T_{2y}(t_i) - \frac{1}{2}f_2K_{21}(t_i)}{T_{2x}(t_i) + \frac{1}{2}e_2K_{21}(t_i)}\right) \\
\phi_3(t_i) &= \arctan\left(\frac{T_{1y}(t_i) - d_1K_{11}(t_i)}{T_{1x}(t_i) - \frac{1}{2}e_1K_{11}(t_i)}\right) & \phi_9(t_i) &= \arctan\left(\frac{T_{2y}(t_i)}{T_{2x}(t_i) - \frac{1}{2}e_2K_{21}(t_i)}\right) \\
\phi_4(t_i) &= \arctan\left(\frac{T_{1y}(t_i) - d_1K_{11}(t_i)}{T_{1x}(t_i) + \frac{1}{2}e_1K_{11}(t_i)}\right) & \phi_{10}(t_i) &= \arctan\left(\frac{T_{2y}(t_i)}{T_{2x}(t_i) + \frac{1}{2}e_2K_{21}(t_i)}\right) \\
\phi_5(t_i) &= \arctan\left(\frac{T_{1y}(t_i) + (\frac{1}{2}f_1 - d_1)K_{11}(t_i)}{T_{1x}(t_i) - \frac{1}{2}e_1K_{11}(t_i)}\right) & \phi_{11}(t_i) &= \arctan\left(\frac{T_{2y}(t_i) + \frac{1}{2}f_2K_{21}(t_i)}{T_{2x}(t_i) - \frac{1}{2}e_2K_{21}(t_i)}\right) \\
\phi_6(t_i) &= \arctan\left(\frac{T_{1y}(t_i) + (\frac{1}{2}f_1 - d_1)K_{11}(t_i)}{T_{1x}(t_i) + \frac{1}{2}e_1K_{11}(t_i)}\right) & \phi_{12}(t_i) &= \arctan\left(\frac{T_{2y}(t_i) + \frac{1}{2}f_2K_{21}(t_i)}{T_{2x}(t_i) + \frac{1}{2}e_2K_{21}(t_i)}\right)
\end{aligned} \tag{6}
$$

New calculations are made in this paper to determine the hitch angles between truck and first trailer and first and second trailers. Hitch angles were not calculated in the algorithm of [8]. The central axis through the hitch point of the truck, from back to front, is described by the tangent vector to the path of (x, y), which is $\mathbf{t} = \cos(\theta(t_i))\,\mathbf{i} + \sin(\theta(t_i))\,\mathbf{j}$, and the central axis through the hitch point of the first trailer and the truck, from back to front, is described by the vector $\mathbf{t_1} = (x_1(t_i) - x_2(t_i))\,\mathbf{i} + (y_1(t_i) - y_2(t_i))\,\mathbf{j}$. Properties of the vector cross product can be used to determine the angle $-\frac{\pi}{2} \leq \varphi_1 \leq \frac{\pi}{2}$ between these two vectors. The properties we use are that for any vectors $\mathbf{a}$ and $\mathbf{b}$ the magnitude (length) $\|\mathbf{a} \times \mathbf{b}\| = \|\mathbf{a}\|\|\mathbf{b}\| \sin\varphi$ and that $\mathbf{a}$, $\mathbf{b}$ and $\mathbf{a} \times \mathbf{b}$ form a right handed set. Since we are dealing with vectors in the $\mathbf{ij}$ plane, their cross product will always be a scalar multiple of the standard third dimension vector $\mathbf{k}$ perpendicular to the plane, so that φ_1 will be positive for anticlockwise rotation and negative for clockwise (see Figure 6).

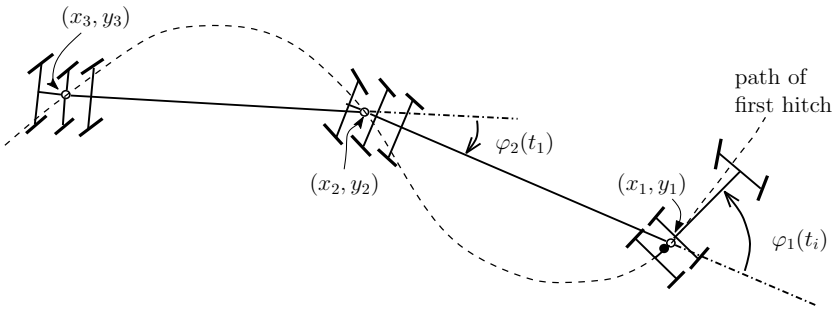

Figure 6: Hitch angles

The same method is used to calculate the hitch angle, φ_2, between the first and second

trailers.

$$\varphi_1(t_i) = \arcsin\left(\frac{(y_1(t_i)-y_2(t_i))\cos(\theta(t_i))-(x_1(t_i)-x_2(t_i))\sin(\theta(t_i))}{\sqrt{(x_1(t_i)-x_2(t_i))^2+(y_1(t_i)-y_2(t_i))^2}}\right)$$

$$\varphi_2(t_i) = \arcsin\left(\frac{(x_1(t_i)-x_2(t_i))(y_2(t_i)-y_3(t_i))-(y_1(t_i)-y_2(t_i))(x_2(t_i)-x_3(t_i))}{\sqrt{(x_1(t_i)-x_2(t_i))^2+(y_1(t_i)-y_2(t_i))^2}\sqrt{(x_2(t_i)-x_3(t_i))^2+(y_2(t_i)-y_3(t_i))^2}}\right)$$

3 Results and discussion

The simulations performed used the dimensions of the B-double shown in Figure 1. The operator is simulated by external functions of front wheel angle and velocity. These functions are sampled at the start of each calculation loop.

The first simulations show the effectiveness of the algorithm applied to B-double truck-trailers. In these simulations the operator steers straight ahead ($\alpha = 0$ in Figure 2) for 9 s then moves into a linearly increasing right turn for 2 s stabilizing at a right turn of $\alpha = -\frac{\pi}{6} = -30^\circ$ held for 5 s. The operator then linearly changes, over 4 s, to a left turn of $\alpha = \frac{\pi}{8} = 22.5^\circ$ which is held for 4 s after which the steering straightens out linearly over a period of 2 s and then remains straight until the 30 s simulation is complete.

We simulate a constant acceleration of 0.2 m/s^2 so the velocity increases linearly as $v = 0.2t$ m/s. Thus, the B-double makes a standing start and increases to a final speed of approximately 21.6 km/h.

Ten simulation runs using $\Delta t = 0.005$ gave an average CPU time of approximately

$0.2\Delta t$ (on a laptop with *Windows* XP operating system, 2.96 GB RAM, processor speed 2.53 GHz) so that the sampling time is 5 times the average calculation time. The calculating time decreases as the path becomes straighter so this particular choice of path requires a great deal of calculation per loop. This is an arbitrary choice of Δt which could have been chosen to be smaller to reduce errors due to discretizing the algorithm. However, for any computational machine there will be a limit to calculating speed and associated errors. In this paper we examine the errors involved in the algorithm when $\Delta t = 0.005$ s with one comparison of wheel angle errors for $\Delta t = 0.001$ s.

Figure 7 shows the hitch path under the given operator specifications. The second hitch starts at (-8.17,0), the third hitch at (-17.52,0) and the truck hitch starts at (0,0), but all hitches follow the same path (as they are, in fact, prescribed to do so). The second and third hitches also finish behind the truck hitch but this is not clearly apparent in Figure 7 since these paths are covered by the truck hitch path. Figure 7 shows the expected path of the hitches given the operator parameters. The truck hitch starts straight then transforms into a circular arc to the right. The hitch path then smoothly changes to a constant circular arc to the left before finally straightening out. The duration of time spent on the second circle is 5 s and that spent on the first 4 s yet approximately twice the arc of circle is navigated on the second circle because the truck is moving with ever increasing speed.

Comparison of the discretized path to analytical solutions are difficult. Equations (1) will at best be approximated numerically as they do not have analytical solutions with the prescribed α and v used in this simulation. We can see, however, the path is straight

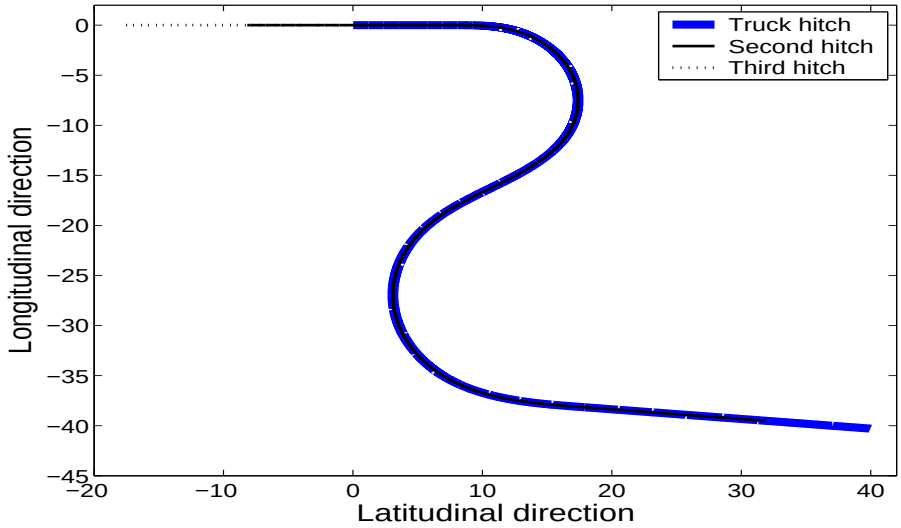

Figure 7: Hitch paths with $\Delta t = 0.005$ s

where it should be and has a radius approximately equal to the analytic radius of curvature of 7.41 m and 10.33 m, on the regions of constant curvature. A closer examination will be made of the wheel angle errors on the regions of constant curvature and also on the determination of the position of the second and third hitch points.

The second hitch point should $l_1 = 8.170$ m behind the truck hitch, and the third hitch point should be $l_2 = 9.350$ m behind the second. Figure 8 shows a plot of the difference between the calculated inter-hitch distances and l_1 or l_2 respectively. Thus it shows the error in locating the exact position of the hitches on the path. The mean of the l_1 error is -1.2508×10^{-6} m and the mean of the l_2 error is 5.1867×10^{-5}, both of which are minute compared to l_1 or l_2, demonstrating that, on average, the error is negligible. The "wobbling" effect of oscillating between negative and positive error is due to the selection

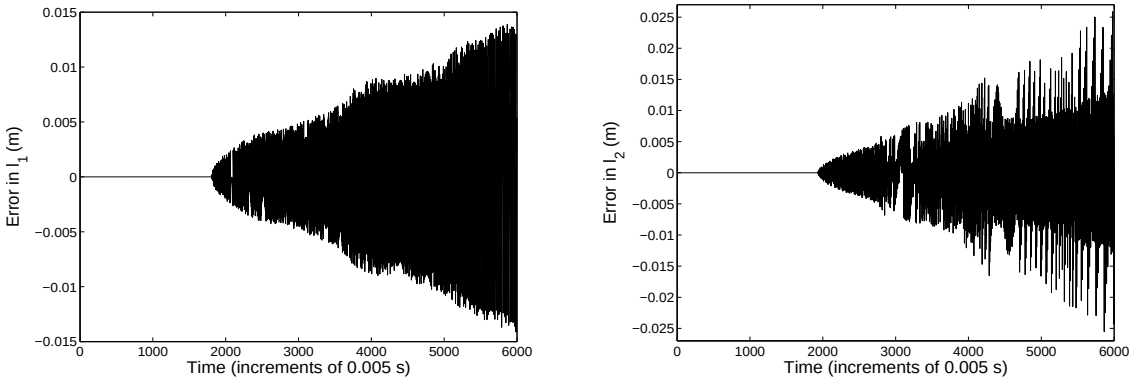

Figure 8: Inter-hitch length errors with $\Delta t = 0.005$ s

of points alternately changing from being closer to further than the actual distance as the algorithm makes its choice of the closest path point to the correct distance. Also clear from Figure 8 is that the error increases with increasing speed because the discrete hitch path points are spaced further apart as speed increases for any fixed Δt.

The initial regions show zero error. This is because the position of the second and third hitches must be calculated using the first hitch and the assumption of a straight path until enough discrete path points are generated for those two trailing hitches. Hence until the second hitch passes the origin it is given as $(x_2(t_i), y_2(t_i)) = (x_1(t_i) - l_1, 0)$ and the third hitch by $(x_3(t_i), y_3(t_i)) = (x_2(t_i) - l_2, 0)$.

Figure 9 graphs the trailer wheel angles as a function of time and shows the large scale pattern of wheel angles that is expected. All wheels start going straight with angle 0, then increase (turn anti-clockwise) before reaching a period of sustained constant angle whilst traversing the circular arc to the right. Of course, throughout the simulation, the

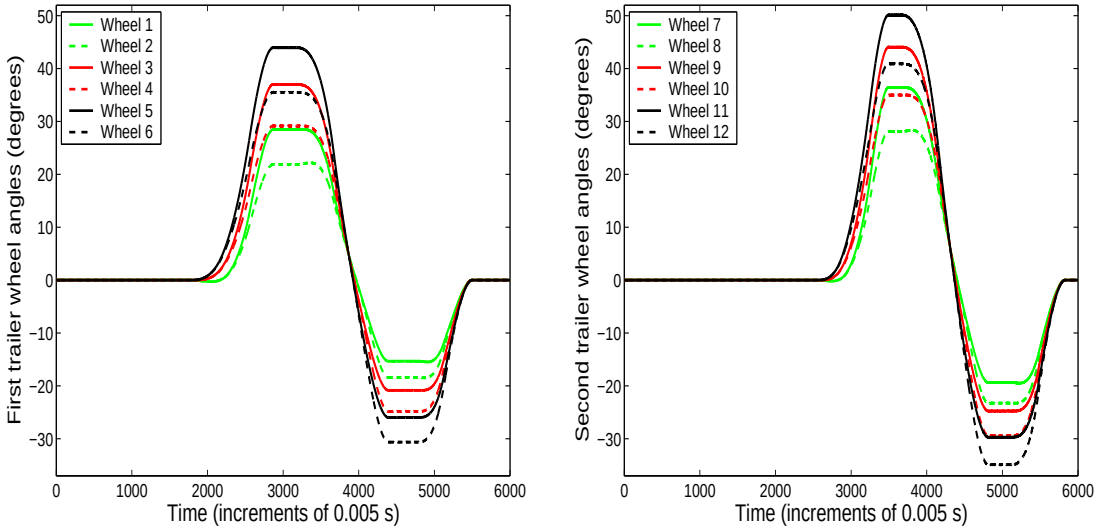

Figure 9: Wheel angles of first and second trailers

second trailer wheels start turning later than the first trailer's because the second trailer is following the first.

On both the first and second trailers the front wheels turn a smaller angle than the middle wheels which turn a smaller angle than the rear wheels. This is as expected since the distance of these wheels, in the direction of the central spine of the trailer is increasingly further from the COC. A scale drawing of Figure 4 would make this perfectly clear. Also, the wheels on the second trailer turn through a larger angle than their corresponding wheels on the first trailer, when traversing the same circle. This is because the interhitch length of the first trailer is 8.170 m whereas the interhitch length of the second trailer is 9.350 m making the COC further from the second trailer wheels in the direction of the central spine of that trailer. In Figure 9 all wheels then change to a constant clockwise angle

(approximately 0.75 times the size of the anticlockwise angles) and finally straighten. We also notice that wheel pairs interchange which angle is largest depending on clockwise or anticlockwise turn because they change being inner or outer wheels in the turns of different direction.

It is not possible to calculate analytical values of wheel angles throughout the simulation. However, it is possible to verify the accuracy of the algorithm for wheel angles in stable regions when two hitch points are on a constant circular path. By trigonometry we can calculate that on the constant right turn with $\alpha = \frac{\pi}{6}$, Wheel 1 should have an angle of 28.470 degrees and for $\alpha = \frac{\pi}{8}$, Wheel 1 should have an angle of -15.329 degrees. Figure 10 contrasts the algorithm calculated wheel angle values with the constant analytical value on these two circular arcs. On both arcs it is clear that there is a wobble in angle in the

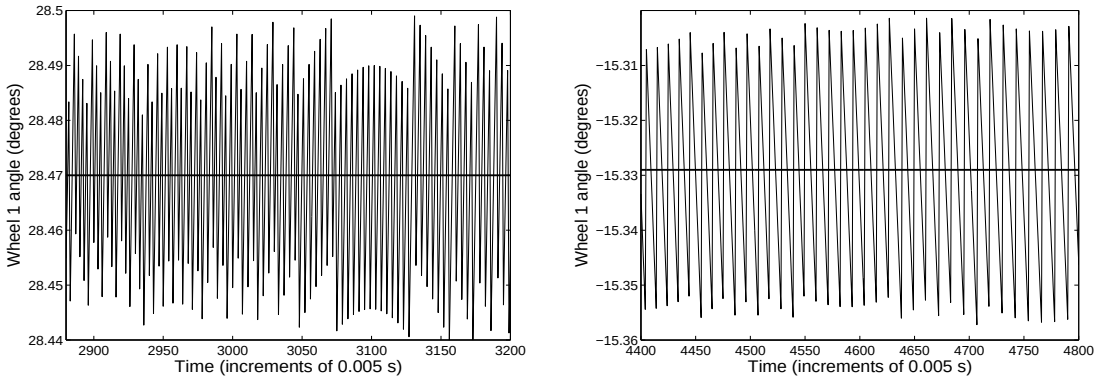

Figure 10: Wheel 1 angles, with $\Delta t = 0.005$ s, compared to the constant analytical value

algorithm calculated value due to the same wobble occurring in Figure 8. We see that the central tendency or mean angle is approximately the analytically calculated value in both

cases. We also notice less wobble in the right hand graph which is caused by the increased speed at that time, spacing the discrete path points further apart and resulting in more choices of path point of the same sign of error (positive or negative) before changing. The change in values of the same sign are difficult to detect at this scale but at larger scales show as jagged sections of the slopes of the angle graph. Although also difficult to detect, this property is also present in Figure 8; look at the spacing between maximal peaks.

To demonstrate that the numerical algorithm converges to the analytical solution as $\Delta t \to 0$ the simulation was run with $\Delta t = 0.001$ s and the resulatant decraese in error shown in Figure 11. The maximal error with $\Delta t = 0.001$ s is approximately 0.005 degrees whereas with $\Delta t = 0.005$ s the maximum error was approximately 0.03 degrees. The mean wheel angle is still approximately the analytical value.

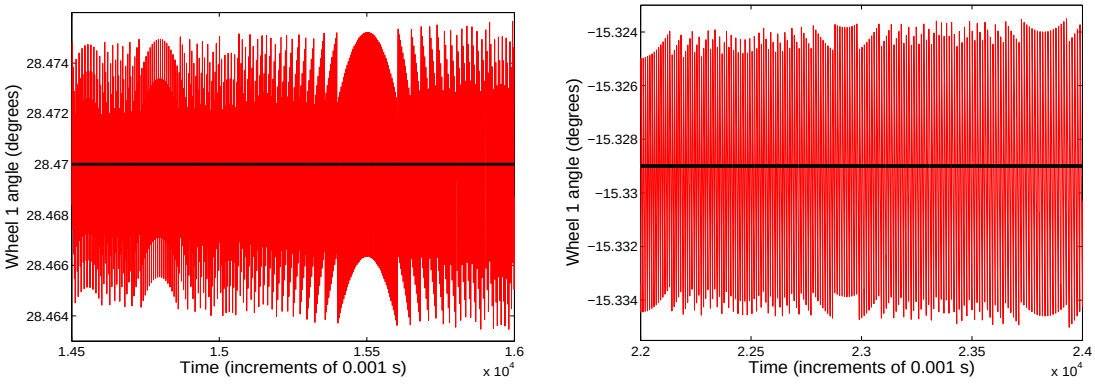

Figure 11: Wheel 1 angles, with $\Delta t = 0.001$ s, compared to the constant analytical value

Figure 12 (left diagram) gives a close up view of four of the wheel angles during the first transition from a straight path to one of constant curvature. The large scale graph of wheel

angles in Figure 9, over the full 30 s period, does not allow the small time scale differences in trailer wheel steering to be observed. The closer examination of Figure 12 (left diagram)

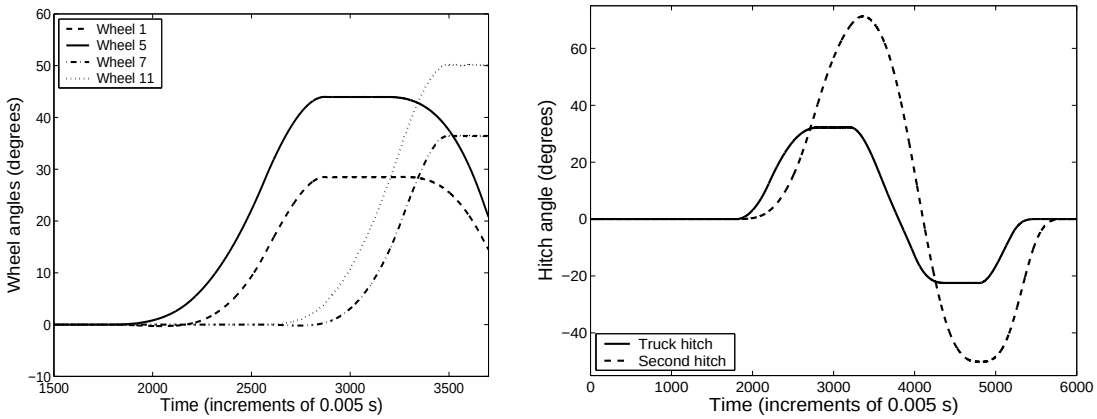

Figure 12: Comparison of wheel angles of first and second trailers (left diagram) and the controlled first and second hitch angles (right diagram)

strengthens the evidence that the algorithm provides the correct wheel angles. Here it is clear not only that the second trailer wheels start turning a short time following the first trailer but also the front wheel of each trailer starts turning before the rear wheel of the trailer for the same reason; that the rear wheel follows the front.

The second (cooperatively redundant) steering system is the controlled hitch angles for this path. These hitch angles are shown in Figure 12 (right diagram). The interesting feature of Figure 12 (right diagram) is the greater hitch angle of the second hitch compared to the truck hitch when the trailers traverse circular arcs. An inspection of Figures 2 and 6 make it clear that the truck hitch angle is the angle formed between the tangent to the

circle and a chord of the circular arc, whereas the second hitch angle will be a greater angle formed by two chords of the circle. This also explains why the second hitch has no periods of constant angle on the first circular arc and a short constant period on the second; because the radius of curvature is sufficiently small that the three hitch points are never on an arc of constant curvature in the first circular arc and only briefly in the second. The first hitch angle being constant only requires the truck and second hitch points to be on a constant arc. It is also noticeable that the second hitch changes angle at a lag behind the truck hitch, again because the second hitch follows the truck hitch by the length of the first trailer.

A second simulation study was conducted to compare the off-tracking of the steered trailer wheels proposed in this paper and standard fixed trailer wheels such as those of the B-double in Figure 1. The operator parameters in this simulation are for a path of constant radius (with $\alpha = -\frac{\pi}{8} = -22.5^\circ$) after an initial linear change from a straight path. Speed increases linearly to 10 m/s (approximately 36 km/h) during the first 10 s and then remains constant for the 13 s simulation.

Figure 13 compares off-tracking of trailers with steered wheels and those with fixed wheels. In particular the wheel paths of wheel 1 of the first trailer (in the left diagram) and wheel 7 of the second trailer (in the right diagram) are shown. The displacement of the second and third hitch points of the fixed wheel trailers (and consequently their wheels) was calculated using the average of the displacement of the truck hitch in the direction of the line joining the second hitch at time t_{i-1} to the front hitch at times t_{i-1} and t_i. At the

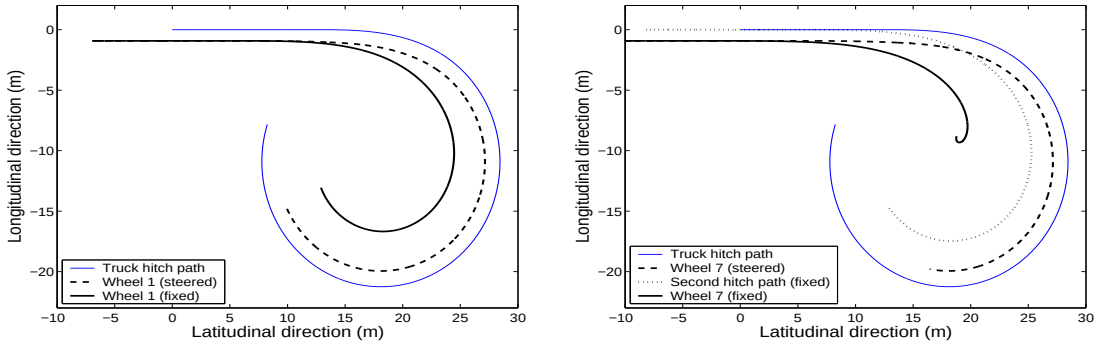

Figure 13: Off-tracking of wheel 1 on the left diagram and wheel 7 on the right diagram of a steered wheel and fixed axis trailer system

small time increment of $\Delta t = 0.005$ s, this average displacement returns a position for the second and third hitches which are within 0.0005% of the true distance from the preceding hitch point.

It is apparent that the off-tracking of the steered trailer wheels are small compared to those of the fixed wheel trailers. It is also apparent that both steered trailers have approximately the same amount of off-tracking, the extent of which is determined by the length of the trailer. The figures show that once a constant curvature is reached, the entire steered trailer system tracks inside the second hitch point of a fixed axle trailer which is itself significantly inside the second trailer wheels of the fixed wheel system. In fact, the right hand diagram shows that a turning angle of $\alpha = -\frac{\pi}{8}$ is too sharp for the fixed axle trailer to perform and the simulation ends with the second hitch pushing the third hitch and Wheel 7 backward. As the number of trailers increase this effect will become greater

for fixed axle trailers whereas any number of the steered trailers will all track closely to the hitch path even in very sharp cornering.

4 Conclusion

Inspection of the simulation studies in Section 3 show that the algorithm for steering multiple trailer vehicles not only appears to be accurate but also of great benefit in terms of reduced off-tracking compared to standard fixed wheel trailers. Compared to analytical solutions we see the discrete numerical algorithm has a "wobbling" effect which could be dampered either in the control system process or simply attenuated by the selection of actuator for wheel angle. The simulations show how the algorithm converges to an analytic real time solution as $\Delta t \to 0$.

The great benefit of steerable trailers is the reduction of off-tracking and scuffing. Such steerable trailers could negotiate corners without the need to swing the truck out across the road into the lanes of on-coming traffic. The use of actively controlled hitch angles provides cooperative reinforcement of the steering system, a back-up if the wheel steering fails and can be used to prevent jack-knifing.

As more trailers are added behind a truck, the advantage of steered trailer wheels become more and more pronounced, so, as the length of road trains increases, so too do the benefits of steerable trailer wheels and actively controlled hitch angles.

References

[1] E. Slawiñski, V. Mut, and J. F. Postigo. Teleoperation of mobile robots with time-varying delay. *Robotica*, 24:673 – 681, 2006.

[2] Lu Liquin and Zhao Jing. The variation law of main parameters on hydraulic steering of articulated dump truck. In *2010 third international conference on Information and computing (ICIC)*, volume 4, pages 316 – 319, Changsha, China, 2010.

[3] Zhiguo Zhao and Jiansheng Wang. Fuzzy optimal design of articulated dump truck's steering mechanism. In *2011 International Conference on Consumer Electronics, Communications and Networks (CECNet)*, pages 4093 – 4096, Xianning, China, 2011.

[4] S. Haggag, D. Alstrom, S. Cetinkunt, and A. Egelja. Modeling, control, and validation of an electro-hydraulic steer-by-wire system for articulated vehicle applications. *IEEE/ASME Transactions on Mechatronics*, 10(6):688 – 692, 2005.

[5] I. J. Spark and M. Yousef Ibrahim. Integrated mechatronics solution to maximize tractability and efficiency of wheeled vehicles. In Bruno Siciliano, editor, *IEEE/ASME International Conference on Advanced Intelligent Mechatronics*, pages 320 – 325, Como, Italy, July, 2001.

[6] I. J. Spark and M. Yousef Ibrahim. Manoeuvrable gantry tractor comprising a chorus line of synchronised modules. *IEEE International Symposium on Industrial Electronics*, pages 2208 – 2213, 2007.

[7] A. Percy, I. J. Spark, and M. Yousef Ibrahim. On-line determination of wheel angles and speeds for manouverable gantry tractor comprising a "chorus line" of synchronised modules. In *IEEE-ICIT'09 International Conference on Industrial Technology*, pages 320 – 325, Churchill, Australia, February, 2009.

[8] A. Percy, I. J. Spark, and M. Yousef Ibrahim. A numerical control algorithm for navigation of an operator driven snake-like robot with 4WD-4WS segments. *Robotica*, 29:471–482, 2011.

[9] G. Campion, G. Bastin, and B. D'Andrea-Novel. Structural properties and classification of kinematic and dynamic models of wheeled mobile robots. *IEEE Transactions on robotics and automation*, 12(1):47 – 61, 1996.

[10] Q. Han and L. Dai. A non-linear dynamic approach to the motion of four-wheel-steering vehicles under various operation conditions. In *Proceedings of the Institute of Mechanical Engineers, Part D: Journal of automobile engineering*, volume 222, pages 535 – 549, 2008.

[11] H. Itoh, A. Oida, and M. Yamazaki. Numerical solution of a 4WD-4WS tractor turning in a rice field. *Journal of terramechanics*, 36:91 – 115, 1999.

[12] Shou-Tao Peng. On one approach to constraining the combined wheel slip in the autonomous control of a 4WS4WD vehicle. *IEEE Transactions on control systems technology*, 15(1):168 – 175, 2006.

[13] I. Waheed and R. Fotouhi. Trajectory and temporal planning of a wheeled mobile robot on an uneven surface. *Robotica*, 27:481 – 489, 2009.

[14] I. J. Spark and M. Yousef Ibrahim. Cooperative redundant steering/drive system: Mechatronic correction for slip angles and longitudinal slip. In *Proceedings of the IEEE International Conference on Mechatronics*, pages 451 – 456, Budapest, Hungary, July, 2006.

[15] I. J. Spark and M. Yousef Ibrahim. Slip angles and longitudinal slip measurement of the cooperative redundant steering/drive system. In *Proceedings of the IEEE International Symposium on Industrial Electronics*, Montreal Canada, July, 2006.

[16] M Lipschutz. *Theory and problems of differential geometry.* McGraw-Hill, 1969.